Letter

Foamlike properties in networks of bundled semiflexible polymers

Lukas P. Weise, Tobias A. Kampmann, and Jan Kierfeld*
Physics Department, TU Dortmund University, 44221 Dortmund, Germany

(Received 27 May 2025; accepted 30 December 2025; published 5 February 2026)

We simulate large systems of mutually attractive semiflexible polymers such as actin filaments in quasi-two dimensions with recently developed event-chain Monte Carlo and molecular dynamics techniques. An isotropic initial state generically evolves into a network of bundles of polymers, which slowly coarsens over time. This explains why networks of bundles are frequently observed in cytoskeletal systems, although one single polymer bundle appears to have a lower free energy. The resulting structure aims to minimize the overall bundle length, which gives rise to properties reminiscent of foams. We apply laws and relations characterizing the structure of foams to the polymer bundle networks. While the empirical Feltham law, as well as the Aboav-Weaire relation, apply to our system, Plateau's law is not followed due to anisotropy and bending stiffness. The coarsening dynamics of the bundle networks are found to be very sensitive with respect to details of the polymer interactions and to deviate from a pure power-law growth of the mean enclosed area, albeit qualitative resemblance to foams remains. We develop a scaling theory capturing the observed coarsening process based on a solidlike friction law for polymer motion in a bundle.

DOI: 10.1103/qrgq-v94k

Introduction. Semiflexible biopolymers such as actin filaments or microtubules serve a variety of purposes in the cytoskeleton: They establish cell shape and mechanics, and they enable active transport and contractile force generation in cooperation with molecular motors, as well as intracellular spatial organization. To fulfill these functions, filaments assemble into a hierarchy of distinct supramolecular structures: Actin can form single filaments, which can assemble into bundles of parallelly aligned filaments (e.g., in filopodia) and into meshed networks of filaments in the actin cortex. While cells induce an effective short-range interfilament attraction via dedicated cross-linking proteins, numerous *in vitro* studies have shown that bundling of actin or microtubule may be effected by generic short-range attractive mechanisms, for example, by counterion condensation or depletion attraction [1–4]. Recently, various synthetic cytoskeletal structures formed by actin or by DNA constructs have been realized, which also employ different short-range attractive interactions for structure formation [5–7].

While a small number of actin filaments with attractive interactions assemble into a single bundle in a well-defined discontinuous phase transition [8], there is mounting evidence from *in vitro* experiments and detailed structural investigations of the *in vivo* actin cortex supporting that large systems of actin filaments assemble into networks of branched actin filament bundles [9–20]. To summarize the main findings of Refs. [16,17], the network structures are insensitive to details of the bundling mechanisms, provided that the attractive interaction is uniform, but depend strongly on the network formation history. After a short timespan, the networks reach a steady state with bundles of finite width, which persists over the experimental timescale. Networks of bundles have also been observed for intermediate filaments [21] and synthetic carbon nanotubes [22].

In this paper, we explore large systems of attractive semiflexible polymers theoretically and show that they generically form coarsening networks of bundles by simulating semiflexible, mutually attractive polymers in a flat three-dimensional (3D) [quasi-two-dimensional (quasi-2D)] volume. The large-scale simulations we perform contain hundreds of polymers and employ recently developed event-chain Monte Carlo (ECMC) techniques [23,24] as well as Langevin dynamics simulations using LAMMPS [25]. As a general consequence of the attraction, the resulting meshed networks aim to reduce their total amount of bundle surface by decreasing the bundle length. For rings formed by a single bundle of semiflexible polymers, this gives rise to a controllable ring contraction [26]. Larger systems of semiflexible polymers associate initially into a network structure, and we find a coarsening of the network of bundles over long timescales, which makes the network of bundles the generically observed state. Only at the end of this long coarsening process, the thermodynamic equilibrium state with a single thick bundle can eventually be reached. This resolves the long-standing question regarding the nature of the equilibrium structure of a simple solution of semiflexible polymers with generic attractive interactions. The long-time coarsening can explain why a structure of networks of bundles is almost universally observed, although one single polymer bundle appears to have a lower free energy. We show that networks of bundles form under generic

*Contact author: jan.kierfeld@tu-dortmund.de

short-range attractive interactions. In the biological literature, emerging cytoskeletal structures are typically attributed to a specific design of actin-binding cross-linkers [27–29], while we find a complex network of bundle structure throughout a long coarsening process without stabilization by specifically designed cross-linkers. Formation of networks of bundles of semiflexible filaments has been reported earlier in simulations of large numbers of attractive filaments [30–33], but their coarsening behavior over long timescales remained unnoticed.

Coarsening is driven by reduction of the total amount of bundle surface and, thus, reduction of the bundle length. This is reminiscent of dry foams where the structure is largely determined by the slow minimization of the area of liquid-gas interfaces. We explore this analogy to foams by applying relations known from foams, such as Plateau's law for angles and Lewis and Feltham laws for the areas and circumferences of network cells. However, the microscopic dynamics of both systems are very different; the bundled networks involve relative sliding of filaments, whereas foams require diffusion of gas through liquid interfaces. We show that this gives rise to a distinct coarsening dynamics in the network of bundles.

Model and simulation. We represent semiflexible polymers using a discrete semiflexible harmonic chain (SHC) model [34]. Each polymer consists of N beads connected by harmonic springs with a spring constant k and a bending energy derived from the bending angle of three neighboring beads with a bending stiffness κ:

$$E_{\mathrm{shc}} = \frac{k}{2}\sum_{n=1}^{N}(|\mathbf{t}_n| - b_0)^2 + \frac{\kappa}{2b_0}\sum_{n=1}^{N-1}(1 - \hat{\mathbf{t}}_{n+1}\cdot\hat{\mathbf{t}}_n), \qquad (1)$$

where $\mathbf{t}_n = \mathbf{r}_n - \mathbf{r}_{n-1}$ denotes the bond vectors connecting the beads n and $n-1$, $\hat{\mathbf{t}}_n$ is normalized, and b_0 is the bond rest length. Additionally, each bead consists of a hard sphere with diameter σ and an attractive square well (SW) potential with diameter $d = 1.4\sigma$ and strength g corresponding to a two-particle potential $V(r) = V_{\mathrm{hs}}(r) + V_{\mathrm{ad}}(r)$ with $V(r) = \infty$ for $r < \sigma$, $V(r) = -g$ for $\sigma < r \leqslant d$, and $V(r) = 0$ for $r < d$. This potential serves as generic model for various adhesion mechanisms, e.g., counterion-induced attraction, depletion, or specific cross-linking proteins [8], or poor solvents [35]. In this paper, we consider weak binding of polymers, i.e., $g \lesssim k_B T$, and the polymers can slide along each other. Effects like coupled bending known from the wormlike bundle model [36] do not arise. In the simulation, we measure lengths in units of the hard sphere diameter σ, energies in units of $k_{\mathrm{B}}T$, and times in multiples of integration steps Δt (molecular dynamics, MD) or sweeps (Monte Carlo, MC). Values of the interaction parameters are provided in Sec. II of the Supplemental Material [37].

Typical simulation systems consist of hundreds of polymers with several hundreds of beads, which requires an efficient simulation technique. We use the ECMC algorithm, which was successfully applied to a variety of systems [38–42]. For a detailed description, we refer to reviews [23,24]. In short, the ECMC algorithm is a rejection-free Monte Carlo method performing in each event chain a cluster move of many particles. It has been generalized to bead-spring polymer simulations with bending rigidity in Refs. [42,43] and shown to produce a realistic polymer dynamics resembling MD [42]. We compare our ECMC simulations, in particular, the time evolution of our system, to Langevin dynamics simulations performed with the well-established MD package LAMMPS [25]. Since the bead potential $V(r)$ is discontinuous, we also use an attractive Lennard-Jones (LJ) potential in MD and ECMC simulations to facilitate a comparison.

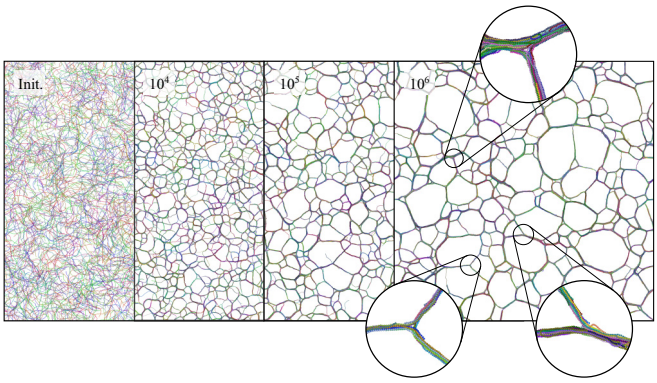

FIG. 1. An isotropically initialized system of 2800 mutually attracting SHC polymers evolves into a meshed network of polymer bundles. Numbers in the upper left corners give the simulation time in sweeps.

Quasi-2D networks of bundled polymers. Simulations are performed in flat, i.e., $L_z \ll L_{x,y}$, three-dimensional volumes with periodic boundary conditions along the x and y directions and hard walls at the z boundaries. Starting from an isotropic initialization and with an attraction g sufficient to induce bundle formation [8], the system of polymers evolves into a meshed network of polymer bundles (see Fig. 1).

The equilibrium properties of similar systems have been examined in several theoretical studies [8,35,44–46]. From the results therein, we expect our system to evolve toward an equilibrium configuration of a single bundle similar to a nematic phase. We find that for sufficiently long and stiff polymers (see Sec. II of the Supplemental Material [37]), this evolution proceeds for a long time via intermediate (network) structures as shown in Fig. 1, which will be typically observed in experiments and are the focus of this study.

The coordination of the bundled network in Fig. 1 is approximately $z \approx 3$; that is, three bundles meet at a *vertex* in accordance with experiments [16]. If the evolution of the network is followed, we observe coarsening via a decrease of the number of meshes and a concomitant growth of the mean mesh area. This behavior is reminiscent of other 2D cellular structures seeking to minimize the overall edge length [47]. A similar driving force governs the network of bundled polymers: The total number of attractive overlaps between beads is increased if the amount of bundle surface in the system is reduced. Therefore, configurations with less and shorter bundles are favored. An important difference of the polymer networks to simple cellular structures like dry soap froths is the non-negligible bending stiffness. To quantify the structural properties and the behavior of the bundled polymer network, we apply an image analysis approach (see Sec. III of the Supplemental Material [37]).

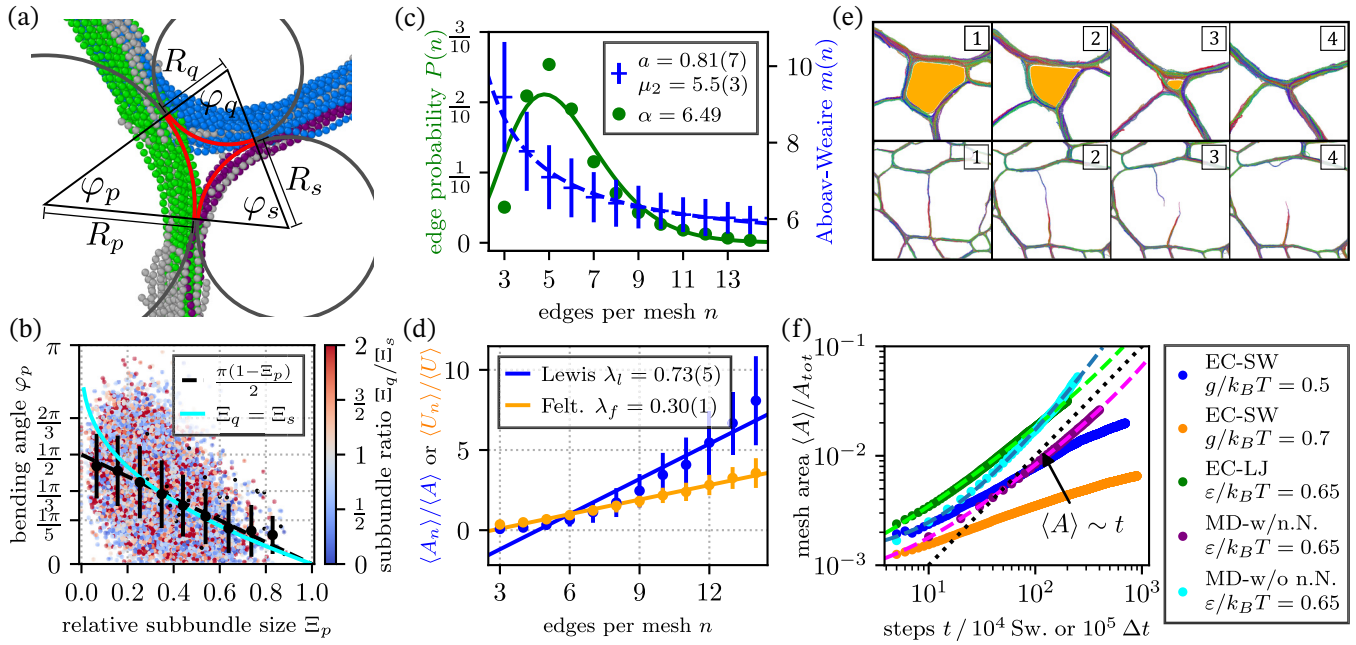

FIG. 2. (a) Sketch of the local vertex model. Red arcs represent the constant curvature approximation of the bundles. The polymers are colored to illustrate the assignment to three subbundles (gray polymers are not assigned to any subbundle). (b) Comparison of the model prediction for $N_q = N_s$ and angles measured from EC-SW $g = 0.7\,k_BT$ network simulations (dots are colored according to the ratio of the subbundle sizes Ξ_q/Ξ_s). All measured angles are assigned to ten bins of width $\Delta\Xi_p = 0.1$ and mean bending angles are computed (black dots). (c) Aboav-Weaire relation $m(n)$ and probability $P(n)$ of observing a mesh with n edges. A gamma distribution is fitted to the edge number histogram (EC-SW $g = 0.7\,k_BT$). (d) Test of applicability of the Lewis $\langle A_n\rangle/\langle A\rangle$ and Feltham laws $\langle U_n\rangle/\langle U\rangle$ on the polymer network (EC-SW $g = 0.7\,k_BT$). (e) Coarsening processes: *Zipping* proceeds by lateral aggregation of bundles (top). In *ripping*, one bundle is torn apart leading to mesh coalescence (bottom). (f) Mean mesh area $\langle A\rangle$ (dots) as a function of the simulation time. The EC-LJ and MD simulations employ a Lennard-Jones pair potential and EC-SW the square well potential. MD-w/o n.N. denotes the system with disabled pair potential for bonded beads. The fits (dashed lines) are computed by integrating (2) and the parameters are provided in Fig. S35 of the Supplemental Material [37]. Coarsening that is asymptotically slower than $\langle A\rangle \sim t$ (dotted black line) is kinetically trapped.

Characteristics of the network structure. We start with an investigation of asymptotic statistical structural properties of the network by averaging over 20–50 simulation runs and compare the results with laws known from dry soap froths.

The *mesh angles* between bundles converging at a vertex are controlled by two competing tendencies. A minimization of the total bundle length gives rise to Plateau's laws; i.e., three edges meet at a vertex at inner angles of $2\pi/3$ (assuming a homogeneous surface tension). It is apparent from Fig. 1 that Plateau's laws are not strictly obeyed. This is in part attributed to differences in the number of polymers per bundle, which effectively translates into inhomogeneous surface tensions. The second, counteracting tendency is the bending stiffness, which favors straight conformations of polymer bundles. That way, a dependence of the angles on the local polymer configuration in the vertex is introduced.

Each vertex is characterized by its relative subbundle sizes Ξ. All polymers that emanate from one bundle and enter the same of the other two bundles at the vertex constitute a subbundle [see colors in Fig. 2(a) or Fig. S9 of the Supplemental Material [37]]. Then, Ξ_u is defined as the number of polymers N_u in subbundle u relative to the total number of polymers traversing the vertex, $\Xi_u \equiv N_u/\sum_j N_j$. To explain the observed mesh angles, we formulate a local model of an isolated vertex as illustrated in Fig. 2(a). A continuum approximation of the subbundles as arcs of constant curvature is applied within the domain of the vertex. Each subbundle is associated with an energy consisting of contributions from decoupled bending $\sim N_u$ and missing attractive overlaps on the surface $\sim\sqrt{N_u}$, $E_u = N_u(\kappa/2)L_u/R_u^2 + \sqrt{N_u}gL_u$, where κ and g control the bending stiffness and the strength of the attractive overlaps, respectively, $L_u = \varphi_u R_u$ denotes the length of the arc, and we approximate each subbundle as cylinder of length L_u and cross-sectional area $N_u\sigma^2$. The vertex shape is determined by a minimization of the total energy $E_V = E_p + E_q + E_s$ of all three subbundles. Angles thus obtained for two symmetric subbundles $\Xi_q = \Xi_s$ are shown in Fig. 2(b) as a function of the relative subbundle size Ξ_p of the third subbundle and compared to measurements taken from polymer network simulations. The details of this calculation as well as additional result for general subbundle sizes $\Xi_q \neq \Xi_s$ are presented in Sec. IV C of the Supplemental Material [37]. Therein, we also substantiate the approximation of subbundles as arcs of constant curvature (Secs. IV B and IV C of the Supplemental Material [37]). A similar local vertex model was formulated in Refs. [31,32] to assign energies to vertices of given bundle sizes and angles.

In the comparison of the isolated vertex model prediction to the actual simulation data in Fig. 2(b), a pronounced scattering of the measured angles is apparent irrespective of the ratio Ξ_q/Ξ_s. This scattering indicates a strong influence of the surrounding network structure onto vertex angles, which

cannot be accounted for in an isolated vertex model. The mean bending angles computed after binning the data with respect to Ξ_p [black dots in Fig. 2(b)] are described very well by a relation linear in Ξ_p (black dashed line). Our model predictions (blue line) are similarly close for all but very small subbundles $\Xi_p \leqslant 0.1$ (see Sec. V C of the Supplemental Material [37]). We also note that Plateau's law $\varphi = \pi/3$ only applies for symmetric vertices $\Xi \approx 1/3$.

Cellular structures in 2D define a tessellation of the plane and are subject to Euler's theorem, which prescribes the mean number of boundaries per cell as $\langle n \rangle = 6$ assuming a vertex coordination of 3. Gamma distributions have been found to provide a good approximation to the distribution $P(n)$ of the number of neighbors in Poisson-Voronoi tessellations [48]. This motivates the choice of a renormalized gamma distribution $P(n) = \lambda^\alpha \Gamma(\alpha, 3)^{-1} n^{\alpha-1} \exp(-\lambda n) \Delta n$ to approximate the histogram of edge numbers [Fig. 2(c)], where the rate parameter λ is determined from the condition $\langle n \rangle = 6$ (see Sec. V D of the Supplemental Material [37]).

An empirical relation known from the context of cellular structures is the *Aboav-Weaire law* $m(n) = 6 - a + (6a + \mu_2)/n$, where a is a parameter and μ_2 denotes the variance of the edge number distribution [49]. The Aboav-Weaire law describes the average number of sides $m(n)$ of cells adjacent to a central cell with n sides. Measurements of $m(n)$ taken from SW simulation data and a fit of the Aboav-Weaire law are shown in Fig. 2(c) (additional data are provided in Fig. S17 of the Supplemental Material [37]). The determined value of a is close to 1 as expected by theoretical arguments [50].

The empirical *Lewis law* $\langle A_n \rangle / \langle A \rangle = \lambda_l (n - \langle n \rangle) + 1$ relates the number of sides n to the conditional mean area of cells $\langle A_n \rangle$ with side number n [51], where λ_l is a free parameter. However, Fig. 2(d) shows that the mean area $\langle A_\mathrm{n} \rangle / \langle A \rangle$ does not scale linearly with n. Correspondingly, the Lewis law is not a very good description and even predicts unphysical negative mean areas for $n \leqslant 4$. The same issue was observed in experimental studies of soap froths [52]. An equivalent to Lewis law that considers the mean circumference $\langle U \rangle$ is the *Feltham law*. It provides a better description of the simulation results compared to Lewis law [Fig. 2(d); additional data are provided in Fig. S18 of the Supplemental Material [37]]. A similar finding was reported in studies of soap froths [53].

Additional structural results on mesh shapes and the number of polymers per bundle are presented in Figs. S14 and S15 of the Supplemental Material [37]. We also show that all structural results are independent of the simulation method (ECMC or MD) and the details of the short-range attraction (SW or LJ).

Coarsening dynamics of the network. The network coarsens toward a configuration of fewer meshes and thicker bundles, while exhibiting invariant distributions of many structural properties (mesh shapes, the number of polymers per bundle, mesh angles, Aboav-Weaire law, and Lewis and Feltham laws; Figs. S14–S18 of the Supplemental Material [37]). This suggests that the bundle network approaches an asymptotic scaling state with statistical self-similarity [54]. However, edge numbers and mesh area distributions hint at deviations from a strict scaling state (Figs. S19 and S20 of the Supplemental Material [37]).

The network coarsening proceeds via two basic processes, zipping and ripping. A *zipping* process, typically initiated by the disappearance of a short edge, is driven by a lateral aggregation of two bundles [Fig. 2(e)] and decreases the area of a mesh continuously. Zipping has also been observed experimentally for networks of actin bundles [16]. It is analogous to bubble disappearance via gas diffusion through the fluid interfaces in foams (T2 process). *Ripping* resembles the coalescence of two foam bubbles by rupture of the fluid interface. Tension from the length minimization of the surrounding network drives polymers within a bundle to slide in opposite directions until the bundle is torn apart [see Fig. 2(e), bottom and Fig. S21 of the Supplemental Material [37]]. Experimentally, the presence of tension in actin bundle networks has been demonstrated by laser cutting [12]. The characteristic timescale of both processes results from the time required for relative sliding of polymers over a bundle length [55]. Similar coarsening modes have been reported in a related simulation study [30] in the limit of weak binding. Zipping processes can be suppressed if polymers are very rigid, and ripping of subbundles can be suppressed if polymers are very long such that they can span entire subbundles and connect neighboring vertices, giving rise to slow impeded coarsening (see also Sec. VII of the Supplemental Material [37]). This is the limit considered in Refs. [31,32], where stable cellular structures without coarsening are found.

The evolution of the *mean mesh area* $\langle A \rangle$ is the most obvious way to analyze coarsening. Of particular interest is the potential existence of a power-law growth regime $\langle A \rangle \sim t^\alpha$, similar to the asymptotic coarsening of a dry 2D foam, where von Neumann's law $\dot{A}_n \propto (n - 6)$ implies $\alpha = 1$ [56,57]. However, the polymer networks are unlikely to obey von Neumann's law because the equilibrium angles are not $2\pi/3$, the boundary properties are not isotropic, and there is no diffusion through interfaces. The mean areas measured across several simulation sets are shown in Fig. 2(f). Interestingly, the coarsening behavior strongly depends on details of the interactions. ECMC simulations with square well pair potential (EC-SW) show a coarsening rate $\langle \dot{A} \rangle$ that *decreases* in time. This gives rise to a prohibitively slow dynamics that is asymptotically slower than $\langle A \rangle \sim t$, prevents the bundle network from reaching the state of a single bundle, and is a strong indication of an evolution toward a kinetically trapped state. An earlier study on bundle formation using a square well to model interpolymer attraction also reports kinetically trapped structures [8]. In contrast, simulations with the soft Lennard-Jones potential (EC-LJ, MD) exhibit unbounded growth, eventually forming a single polymer bundle. A faster coarsening is found in MD simulations (MD-w/o n.N) if the LJ interaction is disabled among first, second, and third nearest-neighbor beads along the polymers. Conversely, a drastic increase in the spring constant or the bending constant combined with an LJ potential leads again to a kinetically trapped state (see Figs. S22 and S23 of the Supplemental Material [37] and Refs. [31,32]). This indicates that details of nearest-neighbor interactions are important for polymer sliding, and kinetic trapping occurs when beads on two neighboring polymers "lock in" [26]. A comparison of MD including nearest-neighbor LJ interactions (MD-w/n.N.) and EC-LJ results shows a surprisingly accurate reproduction of the coarsening by the ECMC algorithm on

long timescales [purple and green dots in Fig. 2(f)] [58]. We find, however, no clear indication of an asymptotic power-law growth.

Toward a more quantitative description of the coarsening process, we use $\langle A\rangle \approx A_{\mathrm{tot}}/N_m$ to relate the mesh area to the number N_m of meshes. Then, the coarsening is linked to the rate of zipping and ripping events R_z and R_r via $\dot{N}_m = -(R_z + R_r)$ resulting in $\mathrm{d}\langle A\rangle/\mathrm{d}t = \langle A\rangle^2(R_z + R_r)/A_{\mathrm{tot}}$. We expect both rates to scale as $R \sim N_m v/L_B$ with the sliding velocity of polymers along the bundles v and an average bundle length L_B; i.e., the event rate is proportional to the number of meshes in the system divided by the characteristic time of edge disappearance (see Sec. X of the Supplemental Material [37]). To gain insight into polymer sliding, we perform simulations of isolated bundles with one of the polymers subjected to an external force and measure the effected displacement along the bundle for different sets of parameters. These simulations indicate a thermally activated overdamped motion with a solidlike friction $v \propto \sinh(CF)$ (see Sec. IX of the Supplemental Material [37]), similar to *in vitro* studies of actin filaments [59]. The parameter $C = \Delta x/k_BT$ is related to the typical distance Δx between energy barriers; the existence of this additional length scale ultimately breaks down asymptotic power-law growth of $\langle A\rangle$. Combining the relation for v with scaling arguments linking the mean bundle length L_B via the mean circumference $\langle U\rangle$ to the mesh area ($L_B \approx \langle U\rangle/\langle n\rangle \sim \langle A\rangle^{1/2}$) and estimating the force as the energy gradient due to the reduction of the total bundle surface ($\langle F\rangle \propto \langle A\rangle^{1/4}$; see Sec. VIII of the Supplemental Material [37]), we obtain a closed time evolution equation for $\langle A\rangle(t)$,

$$\dot{a} = \begin{cases} \hat{b}a^{-1/10}\sinh(\hat{c}a^{1/4})\,, & \text{MD-w/o n.N.,} \\ \hat{b}a^{-17/20}\sinh(\hat{c}a^{1/4})\,, & \text{MD-w/n.N. or EC-LJ,} \end{cases} \tag{2}$$

where $a \equiv \langle A\rangle/A_{\mathrm{tot}}$ and numerical constants $\hat{b}$ and $\hat{c}$. A detailed derivation is provided in Sec. X of the Supplemental Material [37]. Both models allow a good approximation of the simulation data, as shown in Fig. 2(f), confirming the proposed coarsening scenario.

Conclusion. Our large-scale quasi-2D simulations show that semiflexible polymers generically associate into networks of bundles in the presence of isotropic mutual attraction. This structure is not yet in a final thermodynamic equilibrium state but coarsens over long times driven by adhesion energy minimization, which explains the experimental observation of networks of bundles in various systems [9,10,12–17,20–22]. The emerging bundle networks share structural features with foamlike cellular structures, even though Plateau's law ($\theta = 2\pi/3$) is not followed as a consequence of the bending stiffness and nonuniform bundle sizes in the network. The average coordination number is only $z \approx 3$, but Maxwell's rigidity criterion does not apply as vertices are rigidified by polymer bending stiffness. The observed coarsening dynamics is qualitatively similar to foams, while the underlying microscopic processes, adhesive bundle zipping and bundle rupture under adhesion-induced tension, are unique to semiflexible polymer systems and the quantitative behavior generally differs. We could identify several structural properties, which are invariant during coarsening suggesting a state of statistical self-similarity. However, our simulations and empirical scaling arguments do not indicate asymptotic power-law growth of mesh areas and a coarsening dynamics that depends on microscopic details of the interaction between polymer beads, which govern the sliding motion of polymers in a bundle. In reconstituted experimental systems of polymers, a continued coarsening is not observed presumably because of kinetically trapped configurations [12,16], either due to locked polymers that are unable to slide because of cross-linking molecules or by a finite equilibrium bundle width [60,61], which can arise, for example, due to the helical shape of actin filaments [62,63], which is not taken into account in our model. *In vivo*, the ongoing remodeling of the actin networks by (de)polymerization, branching, and eventually pushing forces can further modify the structural properties of the networks of bundles. Nevertheless, networks of bundles remain generically observed structures. The sensitivity of the polymer sliding to details of the interactions is of particular interest for investigations of the mechanical response of bundled polymer networks, where sliding is reported to be one response mode at larger strains [33,64].

The natural extension of our work is the transition to genuine 3D systems [30,33,65–67], which have not been examined with respect to foamlike properties or cellular structure laws so far. Our preliminary results (see Fig. S36 of the Supplemental Material [37]) show networks of polymer bundles that can be viewed as an open-pore foam. Unlike typical open-pore foams, which are generated from area minimization and subsequent removal of cell faces, these structures emerge from edge length minimization as in 2D, making them an interesting subject for future studies.

Acknowledgment. T.A.K. acknowledges funding by the Deutsche Forschungsgemeinschaft (DFG, German Research Foundation) under Grant No. KA 4897/1-1.

J.K. and T.A.K. conceived the study. T.A.K. acquired funding. T.A.K. and L.P.W. designed the simulations. L.P.W. performed and analyzed the simulations. L.P.W. and J.K. conceived the theoretical analysis. L.P.W. and J.K. wrote and revised the manuscript with help of T.A.K.

Data availability. Results of the image analysis, data points for the plots, the analysis code, and the data that supports the findings of this Letter are openly available [68].

[1] B. Alberts, A. Johnson, J. Lewis, M. Raff, K. Roberts, and P. Walter, *Molecular Biology of the Cell*, 5th ed. (Garland Science, New York, NY, 2007).

[2] D. A. Fletcher and R. D. Mullins, Cell mechanics and the cytoskeleton, Nature (London) **463**, 485 (2010).

[3] J. Schnauß, T. Händler, and J. A. Käs, Semiflexible biopolymers in bundled arrangements, Polymers **8**, 274 (2016).

[4] O. Lieleg, M. M. A. E. Claessens, and A. R. Bausch, Structure and dynamics of cross-linked actin networks, Soft Matter **6**, 218 (2010).

[5] P. Zhan, K. Jahnke, N. Liu, and K. Göpfrich, Functional DNA-based cytoskeletons for synthetic cells, Nat. Chem. **14**, 958 (2022).

[6] K. Graham, A. Chandrasekaran, L. Wang, A. Ladak, E. M. Lafer, P. Rangamani, and J. C. Stachowiak, Liquid-like VASP condensates drive actin polymerization and dynamic bundling, Nat. Phys. **19**, 574 (2023).

[7] S. Novosedlik, F. Reichel, T. van Veldhuisen, Y. Li, H. Wu, H. Janssen, J. Guck, and J. van Hest, Cytoskeleton-functionalized synthetic cells with life-like mechanical features and regulated membrane dynamicity, Nat. Chem. **17**, 356 (2025).

[8] J. Kierfeld, T. Kühne, and R. Lipowsky, Discontinuous unbinding transitions of filament bundles, Phys. Rev. Lett. **95**, 038102 (2005).

[9] O. Pelletier, E. Pokidysheva, L. S. Hirst, N. Bouxsein, Y. Li, and C. R. Safinya, Structure of actin cross-linked with α-actinin: A network of bundles, Phys. Rev. Lett. **91**, 148102 (2003).

[10] J. H. Shin, M. L. Gardel, L. Mahadevan, P. Matsudaira, and D. A. Weitz, Relating microstructure to rheology of a bundled and cross-linked F-actin network *in vitro*, Proc. Natl. Acad. Sci. USA **101**, 9636 (2004).

[11] L. S. Hirst, R. Pynn, R. F. Bruinsma, and C. R. Safinya, Hierarchical self-assembly of actin bundle networks: Gels with surface protein skin layers, J. Chem. Phys. **123**, 104902 (2005).

[12] K. M. Schmoller, O. Lieleg, and A. R. Bausch, Internal stress in kinetically trapped actin bundle networks, Soft Matter **4**, 2365 (2008).

[13] K. M. Schmoller, O. Lieleg, and A. R. Bausch, Structural and viscoelastic properties of actin/filamin networks: Cross-linked versus bundled networks, Biophys. J. **97**, 83 (2009).

[14] K. M. Schmoller, P. Fernández, R. C. Arevalo, D. L. Blair, and A. R. Bausch, Cyclic hardening in bundled actin networks, Nat. Commun. **1**, 134 (2010).

[15] S. Deshpande and T. Pfohl, Hierarchical self-assembly of actin in micro-confinements using microfluidics, Biomicrofluidics **6**, 034120 (2012).

[16] S. Deshpande and T. Pfohl, Real-time dynamics of emerging actin networks in cell-mimicking compartments, PLoS One **10**, e0116521 (2015).

[17] F. Huber, D. Strehle, J. Schnauß, and J. Käs, Formation of regularly spaced networks as a general feature of actin bundle condensation by entropic forces, New J. Phys. **17**, 043029 (2015).

[18] I. K. Piechocka, K. A. Jansen, C. P. Broedersz, N. A. Kurniawan, F. C. MacKintosh, and G. H. Koenderink, Multiscale strain-stiffening of semiflexible bundle networks, Soft Matter **12**, 2145 (2016).

[19] Z. G. Sun and M. Murrell, Cofilin-mediated filament softening and crosslinking counterbalance to enhance actin network flexibility, Phys. Rev. Lett. **133**, 218402 (2024).

[20] D. A. D. Flormann, L. Kainka, G. Montalvo, C. Anton, J. Rheinlaender, D. Thalla, D. Vesperini, M. O. Pohland, K. H. Kaub, M. Schu, F. Pezzano, V. Ruprecht, E. Terriac, R. J. Hawkins, and F. Lautenschläger, The structure and mechanics of the cell cortex depend on the location and adhesion state, Proc. Natl. Acad. Sci. USA **121**, e2320372121 (2024).

[21] S. Köster, D. A. Weitz, R. D. Goldman, U. Aebi, and H. Herrmann, Intermediate filament mechanics *in vitro* and in the cell: From coiled coils to filaments, fibers and networks, Curr. Opin. Cell Biol. **32**, 82 (2015).

[22] M. G. Hahm, H. Wang, H. Y. Jung, S. Hong, S.-G. Lee, S.-R. Kim, M. Upmanyu, and Y. J. Jung, Bundling dynamics regulates the active mechanics and transport in carbon nanotube networks and their nanocomposites, Nanoscale **4**, 3584 (2012).

[23] T. A. Kampmann, D. Müller, L. P. Weise, C. F. Vorsmann, and J. Kierfeld, Event-chain Monte-Carlo simulations of dense soft matter systems, Front. Phys. **9**, 635886 (2021).

[24] W. Krauth, Event-chain Monte Carlo: Foundations, applications, and prospects, Front. Phys. **9**, 663457 (2021).

[25] A. P. Thompson, H. M. Aktulga, R. Berger, D. S. Bolintineanu, W. M. Brown, P. S. Crozier, P. J. in 't Veld, A. Kohlmeyer, S. G. Moore, T. D. Nguyen, R. Shan, M. J. Stevens, J. Tranchida, C. Trott, and S. J. Plimpton, LAMMPS—A flexible simulation tool for particle-based materials modeling at the atomic, meso, and continuum scales, Comput. Phys. Commun. **271**, 108171 (2022).

[26] M. Illig, K. Jahnke, L. P. Weise, M. Scheffold, U. Mersdorf, H. Drechsler, Y. Zhang, S. Diez, J. Kierfeld, and K. Göpfrich, Triggered contraction of self-assembled micron-scale DNA nanotube rings, Nat. Commun. **15**, 2307 (2024).

[27] S. J. Winder and K. R. Ayscough, Actin-binding proteins, J. Cell Sci. **118**, 651 (2005).

[28] P. Lappalainen, Actin-binding proteins: The long road to understanding the dynamic landscape of cellular actin networks, Mol. Biol. Cell **27**, 2519 (2016).

[29] L. Blanchoin, R. Boujemaa-Paterski, C. Sykes, and J. Plastino, Actin dynamics, architecture, and mechanics in cell motility, Physiol. Rev. **94**, 235 (2014).

[30] R. D. Groot, Mesoscale simulation of semiflexible chains. II. Evolution dynamics and stability of fiber bundle networks, J. Chem. Phys. **138**, 224904 (2013).

[31] A. Sengab and R. C. Picu, Filamentary structures that self-organize due to adhesion, Phys. Rev. E **97**, 032506 (2018).

[32] R. C. Picu and A. Sengab, Structural evolution and stability of non-crosslinked fiber networks with inter-fiber adhesion, Soft Matter **14**, 2254 (2018).

[33] E. P. DeBenedictis, Y. Zhang, and S. Keten, Structure and mechanics of bundled semiflexible polymer networks, Macromolecules **53**, 6123 (2020).

[34] J. Kierfeld, O. Niamploy, V. Sa-yakanit, and R. Lipowsky, Stretching of semiflexible polymers with elastic bonds, Eur. Phys. J. E **14**, 17 (2004).

[35] J. Midya, S. A. Egorov, K. Binder, and A. Nikoubashman, Phase behavior of flexible and semiflexible polymers in solvents of varying quality, J. Chem. Phys. **151**, 034902 (2019).

[36] C. Heussinger, M. Bathe, and E. Frey, Statistical mechanics of semiflexible bundles of wormlike polymer chains, Phys. Rev. Lett. **99**, 048101 (2007).

[37] See Supplemental Material at http://link.aps.org/supplemental/10.1103/qrgq-v94k for details on the simulation parameters and analysis procedure, figures of structural and dynamical properties of network simulations other than EC-SW $g = 0.7\,k_BT$, derivations, and implementations of the theory presented in the main text, which includes Refs. [69–75].

[38] E. P. Bernard, W. Krauth, and D. B. Wilson, Event-chain Monte Carlo algorithms for hard-sphere systems, Phys. Rev. E **80**, 056704 (2009).

[39] S. C. Kapfer and W. Krauth, Sampling from a polytope and hard-disk Monte Carlo, J. Phys. Conf. Ser. **454**, 012031 (2013).

[40] M. Michel, S. C. Kapfer, and W. Krauth, Generalized event-chain Monte Carlo: Constructing rejection-free global-balance algorithms from infinitesimal steps, J. Chem. Phys. **140**, 054116 (2014).
[41] M. Michel, J. Mayer, and W. Krauth, Event-chain Monte Carlo for classical continuous spin models, Europhys. Lett. **112**, 20003 (2015).
[42] T. A. Kampmann, H.-H. Boltz, and J. Kierfeld, Monte Carlo simulation of dense polymer melts using event chain algorithms, J. Chem. Phys. **143**, 044105 (2015).
[43] J. Harland, M. Michel, T. A. Kampmann, and J. Kierfeld, Event-chain Monte Carlo algorithms for three- and many-particle interactions, Europhys. Lett. **117**, 30001 (2017).
[44] A. Khokhlov and A. Semenov, On the theory of liquid-crystalline ordering of polymer chains with limited flexibility, J. Stat. Phys. **38**, 161 (1985).
[45] R. Chelakkot, R. Lipowsky, and T. Gruhn, Self-assembling network and bundle structures in systems of rods and crosslinkers—A Monte Carlo study, Soft Matter **5**, 1504 (2009).
[46] C. J. Cyron, K. W. Müller, K. M. Schmoller, A. R. Bausch, W. A. Wall, and R. F. Bruinsma, Equilibrium phase diagram of semi-flexible polymer networks with linkers, Europhys. Lett. **102**, 38003 (2013).
[47] C. V. Thompson, Grain growth and evolution of other cellular structures, in *Solid State Physics*, Vol. 55, edited by H. Ehrenreich and F. Spaepen (Academic Press, Cambridge, MA, 2001), pp. 269–314.
[48] S. Kumar and S. K. Kurtz, Properties of a two-dimensional Poisson-Voronoi tesselation: A Monte-Carlo study, Mater. Charact. **31**, 55 (1993).
[49] D. Aboav, The arrangement of cells in a net, Metallography **13**, 43 (1980).
[50] D. Weaire, Some remarks on the arrangement of grains in a polycrystal, Metallography **7**, 157 (1974).
[51] F. T. Lewis, The correlation between cell division and the shapes and sizes of prismatic cells in the epidermis of *Cucumis*, Anat. Rec. **38**, 341 (1928); A comparison between the mosaic of polygons in a film of artificial emulsion and the pattern of simple epithelium in surface view (cucumber epidermis and human amnion), **50**, 235 (1931); The geometry of growth and cell division in epithelial mosaics, Am. J. Bot. **30**, 766 (1943).
[52] J. A. Glazier, S. P. Gross, and J. Stavans, Dynamics of two-dimensional soap froths, Phys. Rev. A **36**, 306 (1987).
[53] K. Szeto and W. Tam, Lewis' law versus Feltham's law in soap froth, Physica A **221**, 256 (1995).
[54] W. W. Mullins, The statistical self-similarity hypothesis in grain growth and particle coarsening, J. Appl. Phys. **59**, 1341 (1986).
[55] For a zipping process to occur, polymers must slide along the bundles so that edges can change their lengths. A bundle is torn apart in a rupture event after the polymers have slid half a bundle length along each other.
[56] J. Stavans, Temporal evolution of two-dimensional drained soap froths, Phys. Rev. A **42**, 5049 (1990).
[57] W. Mullins, On idealized two dimensional grain growth, Scr. Metall. **22**, 1441 (1988).
[58] The horizontal offset is due to the definition of the term "sweep," which we defined as starting one EC for each particle.
[59] A. Ward, F. Hilitski, W. Schwenger, D. Welch, A. W. C. Lau, V. Vitelli, L. Mahadevan, and Z. Dogic, Solid friction between soft filaments, Nat. Mater. **14**, 583 (2015).
[60] G. H. Lai, R. Coridan, O. V. Zribi, R. Golestanian, and G. C. L. Wong, Evolution of growth modes for polyelectrolyte bundles, Phys. Rev. Lett. **98**, 187802 (2007).
[61] L. Haviv, N. Gov, Y. Ideses, and A. Bernheim-Groswasser, Thickness distribution of actin bundles *in vitro*, Eur. Biophys. J. **37**, 447 (2008).
[62] G. M. Grason and R. F. Bruinsma, Chirality and equilibrium biopolymer bundles, Phys. Rev. Lett. **99**, 098101 (2007).
[63] G. M. Grason, Frustration and packing in curved-filament assemblies: From isometric to isomorphic bundles, Soft Matter **9**, 6761 (2013).
[64] C. Wang, B. Xie, Y. Liu, and Z. Xu, Mechanotunable microstructures of carbon nanotube networks, ACS Macro Lett. **1**, 1176 (2012).
[65] M. J. Stevens, Bundle binding in polyelectrolyte solutions, Phys. Rev. Lett. **82**, 101 (1999).
[66] L. T. Nguyen, W. Yang, Q. Wang, and L. S. Hirst, Molecular dynamics simulation of F-actin reveals the role of cross-linkers in semi-flexible filament assembly, Soft Matter **5**, 2033 (2009).
[67] R. J. Pandolfi, L. Edwards, D. Johnston, P. Becich, and L. S. Hirst, Designing highly tunable semiflexible filament networks, Phys. Rev. E **89**, 062602 (2014).
[68] L. P. Weise, T. A. Kampmann, and J. Kierfeld, Foam-like properties in networks of bundled semiflexible polymers [Data set], in Physical Review Research, Zenodo (2026), https://doi.org/10.5281/zenodo.15481844.
[69] E. A. J. F. Peters and G. de With, Rejection-free Monte Carlo sampling for general potentials, Phys. Rev. E **85**, 026703 (2012).
[70] H. Watanabe, N. Ito, and C.-K. Hu, Phase diagram and universality of the Lennard-Jones gas-liquid system, J. Chem. Phys. **136**, 204102 (2012).
[71] V. Popov and J. Gray, Prandtl-Tomlinson model: History and applications in friction, plasticity, and nanotechnologies, J. Appl. Math. Mech. **92**, 683 (2012).
[72] P. G. de Gennes, Reptation of a polymer chain in the presence of fixed obstacles, J. Chem. Phys. **55**, 572 (1971).
[73] O. M. Braun and Y. S. Kivshar, Nonlinear dynamics of the Frenkel–Kontorova model, Phys. Rep. **306**, 1 (1998).
[74] F.-J. Elmer, Avalanches in the weakly driven Frenkel-Kontorova model, Phys. Rev. E **50**, 4470 (1994).
[75] T. A. Kampmann, H.-H. Boltz, and J. Kierfeld, Controlling adsorption of semiflexible polymers on planar and curved substrates, J. Chem. Phys. **139**, 034903 (2013).